

Estimation of regional sea level change in the Pearl River Delta from tide gauge and satellite altimetry data



Lei He^{a,b}, Guosheng Li^{a,*}, Kuo Li^c, Yunqiao Shu^d

^a Institute of Geographic Sciences and Natural Resources Research, CAS, No. 11A, Datun Road, Chaoyang District, Beijing 100101, China

^b Graduate University of Chinese Academy of Sciences, No. 19A, Yuquan Road, Beijing 100049, China

^c Institute of Environment and Sustainable Development in Agriculture, CAAS, 12A, Zhongguancun South Street, Haidian District, Beijing 100081, China

^d Center for Agricultural Resources Research, Institute of Genetics and Developmental Biology, CAS, 286 Huaizhong Road, Shijiazhuang, Hebei 050021, China

ARTICLE INFO

Article history:

Received 17 October 2013

Accepted 24 February 2014

Available online 12 March 2014

Keywords:

regional variations

satellite altimetry

sea level

temporal variations

tide gauges

The Pearl River Delta

ABSTRACT

The present study proposes a reconstruction of regionally consistent sea level anomalies in the Pearl River Delta (PRD) over the period 1959–2011. Spatial empirical orthogonal functions (EOFs) derived from satellite altimetry dataset and the corresponding time series of tide gauge records were combined to generate regional sea level anomalies. Based on these datasets, regionally consistent sea level anomalies (RCSLA) are reconstructed using a dimension-reducing method known as principal components analysis. The results show that the accuracy of reconstruction is sensitive to the number of the available tide gauge records, however no significantly effect of the length of the records is observed. The results also indicate that the EOF reconstruction method addresses issues such as the relatively short-term coverage of satellite altimetry data and the sparse and discontinuous nature of tide gauge records, demonstrating the applicability of this technique in investigation of long-term sea level change. Both river flow and El Niño event have considerable impacts on sea level variability in the PRD.

© 2014 Elsevier Ltd. All rights reserved.

1. Introduction

Sea level is a critical indicator of global climate change, and regional relative sea level is of particular importance in coastal regions with high population density and assets (Parker, 1991; Nerem et al., 2006; Pendleton et al., 2011; Weiss et al., 2011). Accordingly, considerable effort has been devoted to understanding such sea level variations (Nicholls and Cazenave, 2010; Boateng, 2012; Woodroffe and Murray-Wallace, 2012; Hallegatte et al., 2013; Yin et al., 2013). Sea level change is not uniform but varies globally in both rate and amplitude, and some regional sea level changes may be several times larger than the global mean value owing to the effects of local factors (Ryan and Noble, 2007; Karim and Mimura, 2008; Marcos et al., 2012). Therefore, improved understanding of trends in regional sea level variability is essential, both for future sea level projection and for coastal planning and management (Parkinson and McCue, 2011; Bosello et al., 2012).

Three primary datasets are typically used to estimate sea level variability: tide gauge records, satellite altimetry data, and model

data. Models provide more detailed information than observational data in relation to the factors that force long-term sea level change (Chust et al., 2010). However, most advanced models conduct only large-scale (e.g., global) simulations (Penduff et al., 2010; VijayaVenkataRaman et al., 2012), and the application of global models to small-scale study areas results in considerable uncertainty. Observational data from both tide gauges and satellite altimetry are more accurate than model data. Tide gauge datasets represent the longest records of sea surface height relative to coastal benchmarks and have been used extensively in studies of regional sea level variability (Woodworth and Player, 2003; Barbosa and Silva, 2009; Parker, 2013). Nevertheless, tide gauges provide temporally heterogeneous cover and suffer from sparse spatial distributions. By their nature, they are restricted to coastlines and open ocean islands; thus, they cannot adequately represent the open oceans (Holgate and Woodworth, 2004). Since the launch of the TOPEX/Poseidon (T/P) satellite in 1992, which was followed by its successors Jason-1 and Jason-2, sea level has been monitored accurately through satellite altimetry with nearly global coverage and short revisit times (Stanev and Peneva, 2001). However, the major disadvantage of satellite altimetry data is its short-term nature: even the longest continuous record from T/P spans no more than 21 years (Dean and Houston, 2013). Moreover, critical

* Corresponding author.

E-mail address: ligs@igsnr.ac.cn (G. Li).

questions remain regarding the interpretation of such short-term datasets in the context of long-term climate variations. Therefore, recent efforts have focused primarily on exploiting the particular advantages of both tide gauge and altimetry datasets, using a combination of the two in the investigation of long-term sea level change (Church et al., 2006; Calafat et al., 2009; Gomez-Enri et al., 2012).

Most previous studies have adopted approaches using empirical orthogonal functions (EOFs) computed from short-term satellite data with global coverage to interpolate long time series of spatially sparse observations (Smith et al., 1996). For example, Chambers et al. (2002) first employed an EOF reconstruction to identify the response of global sea level variability to climate signals such as the El Niño–Southern Oscillation (ENSO) and the Pacific Decadal Oscillation. Subsequently, other attempts have been made to reconstruct sea level height, often comparing the accuracy of reconstructions using data from different sources (e.g., models and tide gauges) or adopting different methods (e.g., EOF and CEOF) (Calafat and Jorda, 2011; Meyssignac et al., 2011; Hamlington et al., 2012). Though many advances have been made over the past 10 years, issues such as assigning weightings to tide gauges for uneven distributions and the effects of the length of tide gauge records on reconstruction accuracy have yet to be addressed. Accordingly, establishment of a reconstruction method at the regional scale and investigation of the factors affecting reconstruction accuracy are necessary.

The Pearl River Delta (PRD), which is located in southern China and abuts the northern coast of the Pacific, is a low-lying area through which the Pearl River flows into the South China Sea (Huang et al., 2004). The threat of sea level rise is increasing in the region because of the low-lying nature of the land, the increasing population and assets, and the effects of climate change (Hallegatte et al., 2013). Therefore, many studies have been conducted to measure sea level change in the PRD using either models or observations and at both large and small scales (Ren, 1993; Ding et al., 2001; Huang et al., 2004; Feng et al., 2012; Zuo et al., 2013). Accurate estimation of the sea level variations in the PRD region has been impeded by the complex forcing factors, discontinuities in tide gauge records (Huang et al., 2001), and the relatively short-term coverage provided by satellite altimetry data. In particular, previous studies were typically undertaken using either tide gauge records or satellite altimetry data separately or have simply compared estimates obtained using the two datasets. To date, no

previous study has combined these two datasets to overcome at least some of the obstacles to accurate assessment of sea level change.

To address this, the present study attempts to reconstruct regional sea level anomalies (RSLA) during 1959–2011 by combining tide gauge records with satellite altimetry data using the EOF method and the least-squares procedure. A principal components analysis (PCA) of RSLA was conducted to form a sequence of regionally consistent sea level anomalies (RCSLA). This technique allows examination of regional sea level variability in the PRD and may provide potential for investigation of sea level changes in other regions.

2. Datasets and methods

2.1. Tide gauge records

The PRD is bounded by high mountainous zones to the east and west, where the vertical crustal motion is different from that of the plain area. To avoid the effects of this crustal motion, the gently sloping plain (20–24°N, 110–118°E; Fig. 1) was selected as the study area. The tide gauge dataset consists of 17 monthly mean sea level series obtained from two sources. The longest record used was the Zhapo tide gauge record (spanning 1959–2011), which was collected from the Permanent Service for Mean Sea Level (PSMSL), with the Revised Local Reference monthly values normalized to a constant local datum. A further 16 monthly records were provided by the Guangdong Hydrology Bureau. In the present study, all data were adjusted to the reference sea level of the Yellow Sea (1985–present) tide gauge zero. All 17 tide gauges are listed in Table 1, and their locations are illustrated in Fig. 1.

Quality control was performed to check these tide gauge records. First, small gaps in the records (1–2 months) were filled using cubic spline interpolation. Second, the effects of river-runoff which is the main local factor of sea level in the PRD were calculated and removed using a correlation function established between river flow and tide gauge data. Finally, all the tide gauge records were submitted to correlation analysis for inter-station consistency check (Unnikrishnan and Shankar, 2007; Raicich, 2008). The strong relationships were found between pairs of the tide gauge, 75% of the correlation coefficients were greater than 0.7 (98% of them were larger than 0.5), at a significance level of 0.01. All the records passed the check.

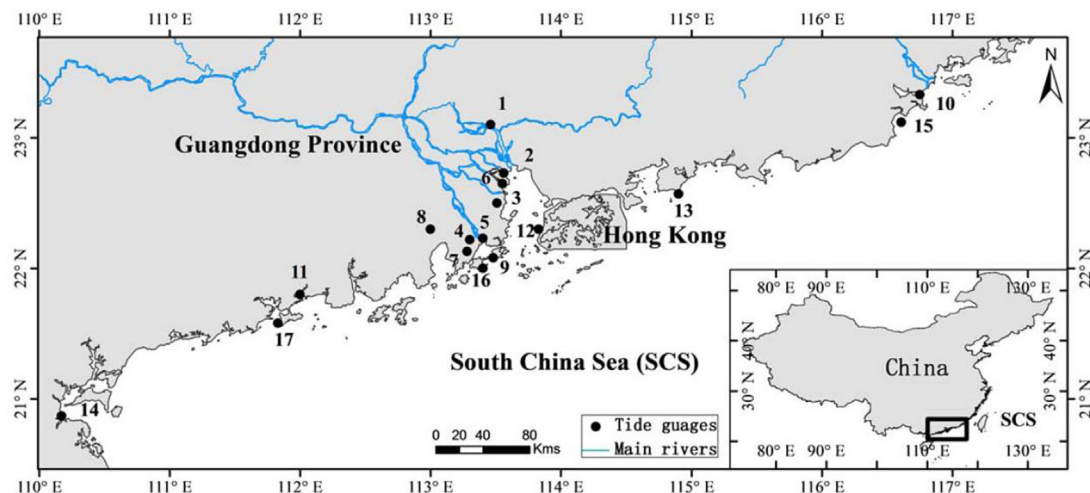


Fig. 1. Location of tide gauges used in the reconstruction.

Table 1
Summary of tide gauge stations used for sea level reconstruction over 1959–2011.

NO.	Tide gauge	Lat.	Lon.	Data valid period	Length (year)
1	Huangpu (HP)	23°06'N	113°28'E	1959–1988 2006–2011	36
2	Nansha (NS)	22°44'N	113°34'E	1963–1988 2001–2005 2007–2011	36
3	Hengmen (HMa)	22°35'N	113°31'E	1959–1988 2001–2005 2007–2011	40
4	Xipaotai (XP)	22°13'N	113°18'E	1959–1965 1974–1988 2001–2005 2007–2011	32
5	Denglongshan (DL)	22°14'N	113°24'E	1961–1988 2001–2005 2007–2011	38
6	Wanqingshaxi (WQ)	22°39'N	113°33'E	1961–1988 2001–2005 2007–2011	38
7	Huangjin (HJ)	22°08'N	113°17'E	1965–1988 2001–2005 2007–2011	34
8	Huangchong (HC)	22°18'N	113°04'E	1961–1988	28
9	Dahengqin (DH)	22°05'N	113°29'E	1979–1988 2001–2005 2007–2011	20
10	Mayu (MY)	23°20'N	116°45'E	1966–1988 2006–2011	29
11	Beijingang (BJ)	21°48'N	112°01'E	1965–1988 2006–2011	30
12	Chiwan (CW)	22°28'N	113°53'E	1966–1988 2006–2011	29
13	Gangkou (GK)	22°34'N	114°54'E	1974–1987 2006–2011	19
14	Nandu (ND)	20°52'N	110°10'E	1964–1987 2006–2011	29
15	Haimen (HMB)	23°12'N	116°37'E	1965–1987 2006–2011	28
16	Sanzhao (SZ)	22°02'N	113°24'E	1967–1986 2001–2005 2007–2011	31
17	Zhapo (ZP)	21°35'N	111°50'E	1959–2011	53

To reconstruct past sea level variability as completely as possible, signals on different timescales (e.g., annual cycles, long-term trends) are typically retained in sea level series. As the present study is concerned only with changes in sea level (rather than absolute sea level), the average sea level height was removed from each tide gauge record and the residual anomalies were used.

2.2. Satellite altimetry dataset

A merged and gridded product of MSLA (Maps of Sea Level Anomaly) produced by AVISO (www.aviso.oceanobs.com) based on T/P, Jason 1, ERS-1/2 and ENVISAT data was used to determine the spatial patterns of sea level change. Combining data from different missions significantly improved estimations of mesoscale signals (Pascual et al., 2006). The altimeter sea surface heights (SSH) measurements have biases and errors that can be very different among missions, and merging multi-satellite altimeter missions requires homogeneous and cross-calibrated SSH data sets (AVISO, 2013). Therefore the most recent corrections, models and references recommended for altimeter products were applied to the data sets, any residual orbit error (Le Traon and Ogor, 1998), or long wavelength error (Le Traon et al., 1998) were removed, as well as large scale biases and discrepancies between various data flows. To extract SLA, a 7-year (1993–1999) mean profile representing the static geoid was subtracted from SSH. Then an optimal interpolation method was applied to the along-track data to obtain the grid SLA. The specific processing of along-track data from the altimetry missions into gridded fields of SLA was described by Le Traon et al. (2003). The MSLA was calculated every 7 days on a $1/3^\circ \times 1/3^\circ$ Mercator grid, the error estimated by AVISO was about 1–2 cm (Niedzielski and Mizinski, 2013). To ensure the temporal consistency with the monthly tide gauge records, weekly maps were statistically downscaled to monthly value. Indeed, intrinsic difficulties affect the corrections applied to the altimeter data within a certain distance of the coastal region (~ 10 km) (e.g., wet tropospheric component, tidal component), many advanced correction and optimal interpretation methods have been developed for it (Mitchum, 2000; Pascual et al., 2006; Bouffard et al., 2011; Escudier et al., 2013). Merging data from multiple missions improved the estimation accuracy of sea level in coastal areas (Ducet et al., 2000; Pascual et al., 2006). MSLA is able to resolve variability on scales as small as 35 km (Ducet et al., 2000; Willis et al., 2004; Siedler et al., 2006), can be a valuable tool to study the sea level variability near the coast (Parker, 1991), several studies have therefore used MSLA data to detect and estimate sea level change (e.g., Isern-Fontanet

et al., 2003; Bi et al., 2011; Niedzielski and Mizinski, 2013). In this study we extracted the monthly gridded MSLA spanning $20\text{--}24^\circ\text{N}$ and $110\text{--}118^\circ\text{E}$ (264 grids) from the global MSLA during 01/1993–12/2011 (19 years) for the reconstruction.

2.3. Reconstruction method

The method used to reconstruct past regional sea level in the PRD is based on the EOF decomposition and PCA described previously by Smith et al. (1996) and Xie et al. (2012), respectively. The method is based on a critical hypothesis that the spatial covariance vectors (also known as EOFs) which represent the dominant spatial patterns of sea level variability deduced from satellite altimetry data are stationary during 1993–2011 in PRD, so that they can be extended to the entire reconstruction period, i.e., 1959–2011.

The first step of the reconstruction involves calculating EOFs from satellite altimetry SLA grid $P(x, t)$, where x represents a given set of grid points and t is time. Then,

$$P(x, t) = \sum_{m=1}^M Z_m(x)L_m(t). \quad (1)$$

Here, Z_m represents the EOFs, L_m represents the related time series of the amplitudes for each time step and M is the number of spatial vectors. Both the EOFs and time weightings are orthonormal and the temporal functions were normalized as follows:

$$\sum_{t=1}^T L_i(t)L_j(t) = \begin{cases} 0 & i \neq j \\ 1 & i = j \end{cases}, \quad (2)$$

and

$$\sum_{x=1}^X Z_i(x)Z_j(x) = \begin{cases} 0 & i \neq j \\ \lambda_i & i = j \end{cases}. \quad (3)$$

Here, X and T are the maximum values of x and t , respectively, and λ is the eigenvalue. The eigenvalues explain the variance associated with each mode and were arranged in descending order. The lower order eigenvectors with the largest eigenvalues explain most of the variance and represent the dominant spatial patterns of the signal. The higher order eigenvectors contain smaller spatial scales and are increasingly affected by noise. For SLA reconstruction, a subset of the eigenvectors, k , that explained the maximum variance with the minimum noise was used.

The second step is fitting the EOFs to the longer spatially correlated tide gauge data to obtain the corresponding amplitudes over 1959–2011. The reconstruction $RSLA(x, v)$, where v represents a time index, was computed by multiplying the EOFs to the time series of amplitudes as follows:

$$RSLA(x, v) = \sum_{m=1}^k Z_m(x)T_m(v), \quad (4)$$

where Z_m represents the EOFs of satellite altimetry SLA and T_m represents the time series of the amplitudes from spatially correlated tide gauge records $Q(x, v)$. The values of x in $Q(x, v)$ and $RSLA(x, v)$ correspond to those in $P(x, t)$. Not all stations could be matched accurately to corresponding spatial grid points for the tide gauge records $Q(x, v)$; therefore, the tide gauges were assigned to the nearest altimetry grid points, letting $\delta(x) = 1$ when a corresponding relationship was found and letting $\delta(x) = 0$ otherwise. Often, several tide gauges were associated with one spatial grid point; in such cases, the available tide gauge records were averaged to produce a single time series. The unknown temporal weights, T_m , were computed by a least-squares procedure, and the function E^2 was defined at each time by

$$E^2(v) = \sum_{x=1}^N [Q(x, v) - RSLA(x, v)]^2 \delta(x), \quad (5)$$

where $E^2(v)$ is the error between the reconstruction and the associated tide gauge records over the entire region at time v . By minimizing E^2 for each T_m , the best fit of the spatial eigenvectors to a given set of data at each time step was obtained. Then, Eq. (4) was

substituted into Eq. (5) and differentiated with respect to T_m to compute the least-squares best fit:

$$\frac{\partial E^2(v)}{\partial T_m(v)} = 0. \quad (6)$$

Then, a set of linear equations was obtained as follows:

$$\sum_{n=1}^k \left[T_m(v) \sum_{x=1}^X Z_n(x)Z_m(x)\delta(x) \right] = \sum_{x=1}^X Q(x, v)Z_m(x)\delta(x), \quad (7)$$

where $m = 1, 2, \dots, k$ represents the first k spatial eigenvectors for reconstruction. T_m was computed for each time step.

The third step is the reconstruction of RSLA. The temporal weights, T_m , were substituted back into Eq. (4) to complete the reconstruction for the period 01/1959–12/2011.

Finally, the RCSLA dataset, a temporal series of SLA with uniform spatial attributes, was obtained by reconstructing the spatial relationship of the RSLA using PCA. The PCA method can extract the important information from many series and express it using fewer principal components (PCs) (Preisendorfer and Mobley, 1988; Cazenave et al., 2002; Barbosa et al., 2005). According to Xie et al. (2012), the components of RSLA, y , can be expressed by PCA as follows:

$$y = \sum_{k=1}^p a_k f_k, \quad (8)$$

where p represents the number of the PCs, f represents a given PC, and a is the associated coefficient.

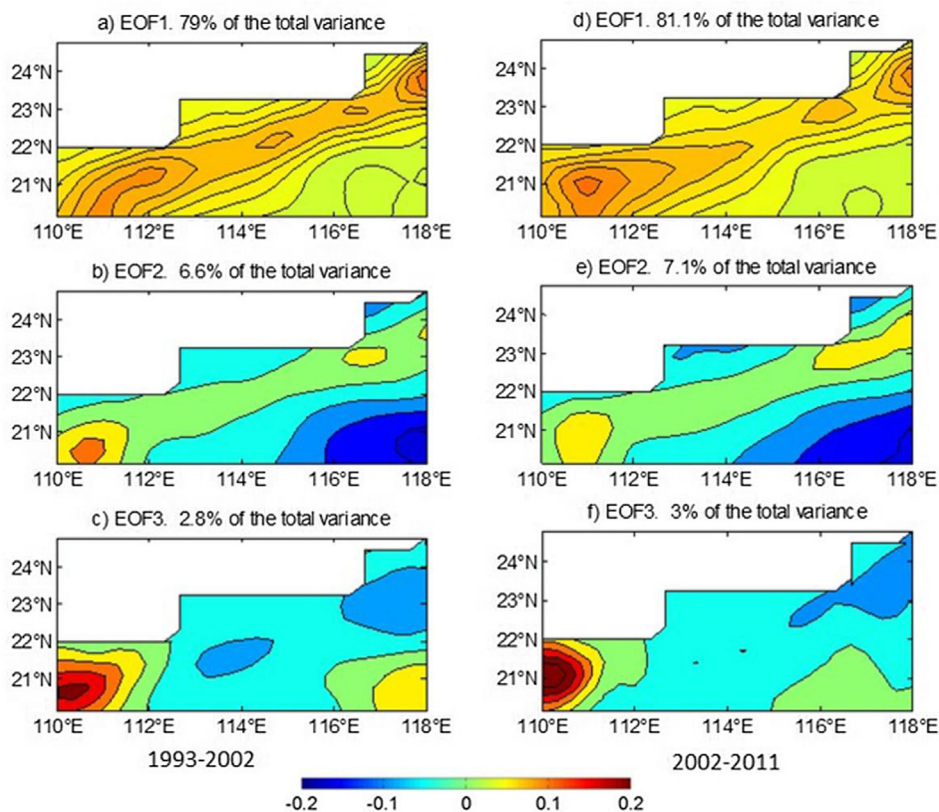


Fig. 2. Comparison of spatial patterns over two periods 1993–2002 and 2002–2011. The first three EOFs of each dataset explaining the largest variance of 79% (a), 6.6% (b), and 2.8% (c) for the first decade and 81.2% (d), 7% (e), and 3% (f) for the last decade, respectively.

When p equals the number of spatial grid points, all of the components are used in reconstruction and Eq. (8) represents the complete information for the series. Usually, the first few components can extract the dominant attributes effectively with lower noise levels than would typically be obtained using all PCs. A weighted average was produced according to the variance contribution rates of the first few components and then obtained the final synthetic RCSLA.

3. Results and discussion

3.1. EOF analysis

To test the consistency of the spatial patterns of sea level variability in the PRD, the satellite altimetry SLA was split into two parts: the first decade, spanning the period 1993–2002; and a later decade spanning the period 2002–2011. Then, spatial SLA patterns for each period, derived by EOF analysis, were compared. The first three EOFs of each dataset are illustrated in Fig. 2 and explain 79%, 6.6%, and 2.8% of the variance for the first decade and 81.2%, 7%, and 3% of the variance for the last decade, respectively. The correlation coefficients (R) between the corresponding EOFs of the two datasets, (a) and (d), (b) and (e), and (c) and (f) are 95%, 97%, and 84%, respectively. These high correlations imply that the dominant spatial patterns for the period 1993–2002 closely resemble those for 2002–2011. The results indicate that the first three EOFs represent the dominant spatial structure of sea level change in the PRD and are stable. This good agreement supports the use of the EOFs calculated from satellite altimetry SLA for the period 1993–2011 in the reconstruction for 1959–2011.

An EOF decomposition of the satellite altimetry data for 1993–2011 was conducted; the dominant EOFs and their correlated time series (with normalized amplitude) are shown in Fig. 3. The

decomposition has a fast convergence rate and the first three modes explain up to 90% of the variance and can abstract the dominant characteristics of the sea level variability. The first EOF explains the majority of the variance (Fig. 3(a), 79.9%) and represents the annual cycle, as shown in Fig. 3(d). Each grid point exhibits the same sign (here taken as positive), implying that the annual variability occurred in the same direction (i.e., increases or decreases); this can be considered the dominant characteristic of sea level variability in the PRD. Moreover, the corresponding time series exhibits a positive trend, with a linear increase of 4.5 mm/yr over the period 1993–2011; this is consistent with the rate estimated for the South China Sea for the period 1993–2006 (3.5 ± 0.9 mm/yr) (Rong et al., 2009). The second EOF, which is characterized by inter-annual variation, exhibits a negative phase in the mouth of the Pearl River but a positive phase in the north-eastern and southwestern parts of the coastline. This pattern demonstrates the strong relationship between sea level, river flow and the backwaters around the mouth of the Pearl River. No such effects were evident in the patterns of sea level variability along the coastline. The third EOF primarily demonstrates the seasonal sea level variability. The evidences of El Niño effects on sea level variation can be observed in all three EOFs. Compared to other years (1993–1996 and 1998–2011), the lowest local maximum is found in the corresponding time series of the first EOF in 1997, when the strongest El Niño event in the 20th century began. Time series of other two EOFs both exhibit obvious abnormal fluctuations during 1997–1998, the highest local maximums are found during that period, respectively. The above analysis are consistent with Ho et al. (2000) who conducted an EOF analysis to study the variation of sea level in the South China Sea and Nerem et al. (1999) who found the global sea level showed a 20 mm rise and then subsequent fall during 1997–1998.

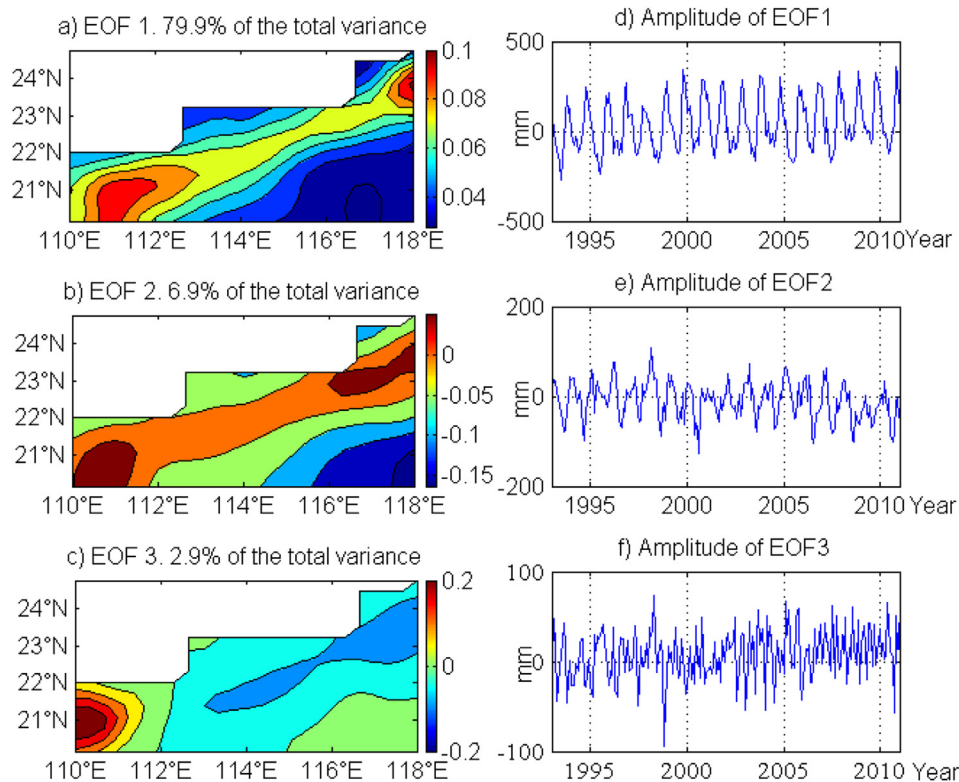


Fig. 3. First three EOFs of satellite altimetry and the corresponding time series. a), b) and c) are EOF1, EOF2 and EOF3, respectively, d), e) and f) are the corresponding time series, respectively.

3.2. Reconstruction of RCSLA

The number of EOFs used is crucial to the reconstruction: using too few EOFs could result in a lack of information regarding the original sea level variability, whereas using too many could induce additional noise. Calafat and Jorda (2011) selected EOFs from 1 to 20 for reconstruction and demonstrated that optimum reconstruction could be achieved using three to four EOFs. We tested the first 2 to 8 EOFs for the reconstruction. The results show that when more than three EOFs were selected, a significant overfitting was occurred. Therefore, the first three EOFs were selected for the PRD SLA reconstruction.

The RSLA were obtained for the period 1959–2011 using EOF decomposition and a least-squares approach. Then PCA was used for dimensionality reduction by expressing the sea level variability in the linear combination of all the reconstructed grid points in RSLA. The first PC explains 62.61% of the total variance and usually represents the dominant pattern of sea level change. The second and third components explain 27.46% and 9.93%, respectively, of the variance. The PCA decomposition has a fast convergence rate and the total contribution of the first three PCs is as much as 99%; thus, using these PCs for RCSLA reconstruction should express the characteristics of RSLA fully. A weighted average was calculated for the PCs and formed a RCSLA series, as shown in Fig. 4.

A decrease in the magnitude of the RCSLA variability can be observed between 1989 and 2005. This could be related to a reduction in the number of available tide gauges between 1989 and 2005. When all the tide gauges were assigned to fit to the corresponding grids in the reconstruction, several tide gauge records were averaged into one, especially for tide gauges near the mouth of the river (e.g., WQ, NS, DL, XP) which have a higher density than those located along coast (e.g., ND, ZP, GK). Finally there were no more than 4 records covering the period of 1989–2005, the least number in the whole reconstruction period. Nevertheless, as we were interested in the long term sea level change in this study, this decrease can have little impact when the high frequency fluctuations (e.g. within 3 years) were removed to get stable estimates of the rate of sea level change (Fenoglio-Marc, 2002; Prandi et al., 2009; Marcos et al., 2012).

3.3. Validation of RSLA

To evaluate the accuracy of the RSLA dataset, it was compared with the SLA of the nearest tide gauges, averaging tide gauge records when more than one tide gauge correlated with a given grid

point. The error statistics calculated are presented in Table 2 (Calafat and Jorda, 2011; Cheng et al., 2012). All of the reconstructions exhibit good estimation performance, with Root Mean Square Error (RMSE) < 0.058 m and coefficient of determination (R^2) > 0.75. All RMSEs (R^2 values) were in the range of 0.0159–0.0573 m (0.758–0.992), with the lowest error (R^2 value) found at the Nandu (Gangkou) tide gauge and the highest at the Gangkou (Nandu) tide gauge. Thus, the Gangkou tide gauge exhibits the highest RMSE and lowest R^2 value, possibly owing to its shortest time series. Zhapo tide gauge is the standard ocean tide gauge in Global Sea Level Observing System (GLOSS), with the longest record covering the whole reconstruction period. Fig. 5 shows the scatter diagram of comparison between the SLAs from Zhapo tide gauge and the nearest gridded reconstruction. From this figure we can see a strong relationship between the observed records and reconstruction value, the correlation coefficient is up to 0.965 and the trend line approximately coincides with that of $y = x$. The comparison represents an encouraging reconstruction result (RMSE = 0.0279 m, $R^2 = 0.947$). The good overall estimation performance, as indicated by the low RMSE (average 0.042 m) and high R^2 value (average 0.878), implies that the reconstruction using EOF decomposition and the least-squares method is applicable for the PRD. Moreover, the results suggest that the method significantly outperforms the multivariate regression approach used by Cheng et al. (2012) who reported the lowest RMSE was 0.05 m, and the reduced optimal interpolation method used by Becker et al. (2012) who obtained some correlation coefficients between 0.5 and 0.7 and Calafat and Jorda (2011) who represented RMSE could be larger than 0.1 m in some region), respectively.

Table 2 also presents the lengths of the compared records: the Zhapo (Gangkou) tide gauge has the longest (shortest) record with 636 (240) samples. A further 8 corresponding records have around 300 samples each, on average. However, differences in the number of samples are not thought to affect the accuracy of the reconstruction. Although the Gangkou tide gauge has both the shortest record and the poorest accuracy, the Zhapo tide gauge exhibits moderate estimation performance (based on RMSE and R^2) despite having the longest record and the Nandu tide gauge exhibits the best performance (RMSE = 0.0159 m) despite using only 360 samples for the reconstruction. Moreover, the number of samples from the Nandu tide gauge can be considered representative of all tide gauges. Thus, the accuracy of reconstruction is not correlated obviously with the length of tide gauge records. This is encouraging, because it indicates that successful reconstruction could be

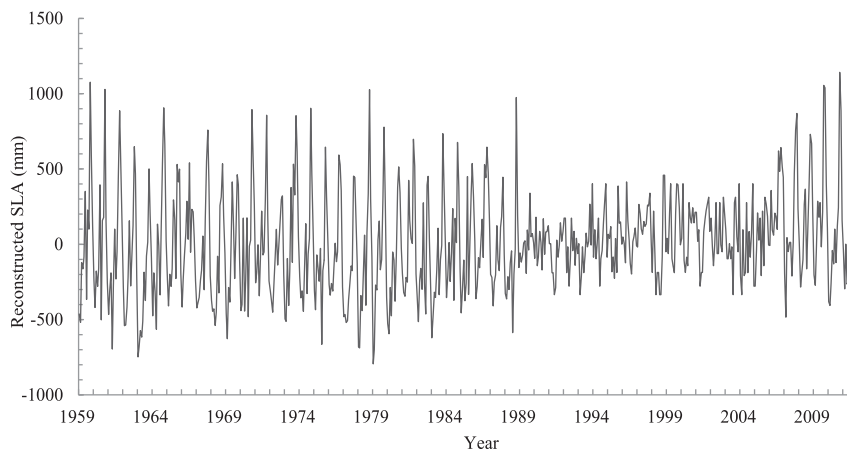


Fig. 4. Regionally consistent sea level anomalies reconstructed by PCA in the PRD.

Table 2
Error statistics of reconstructed sea level anomalies.

Number of the grid points	Name of the tide gauges	Length of the records	RMSE(m)	R ²
1	ZP	636	0.0279	0.9470
2	ND	360	0.0159	0.9924
3	HP	384	0.0312	0.9291
4	HMb/MY	360	0.0489	0.8373
5	GK	240	0.0573	0.7581
6	CW	348	0.0433	0.8477
7	BG	360	0.0562	0.7968
8	HC	300	0.0225	0.7604
9	WQ/HMa/NS	384	0.0291	0.9306
10	DL/XP	384	0.0358	0.9140
11	SZ/DH/HG	360	0.0527	0.7970
Total		4116	0.0423	0.8781

conducted for the coastal area even if only discontinuous or short time series were used.

3.4. Sources of uncertainty

There are three main sources of uncertainty in this reconstruction. First, the method assumes that the leading spatial structures are stationary in time, i.e., that the dominant EOFs of the period 1993–2011 are not very different from those of 1959–2011. It can be proved that in 20 years the variability is stable, but it may be different in a longer period owing to the decadal cycle of sea level change (Latif and Barnett, 1994). Second, the small number of available tide gauge records may cause errors. The number varied each time step due to the nature of the tide gauges, when it was less than 4, a decrease of magnitude in the reconstructed SLA occurred. This may also be related to the distribution of tide gauge. The approach overcomes the sparse and uneven distribution of the tide gauge, whether it can accurately rebuild the signals in the region where there is no any tide gauge nearby is a question need to be investigated further. Finally, the limited number of EOFs used in the reconstruction may result in errors. Only main EOFs were selected implies that the method represents the main variations of sea level, cannot capture the completely attributes. Some small structures may be lost as they tend to be represented by higher order EOFs (not used in the reconstruction).

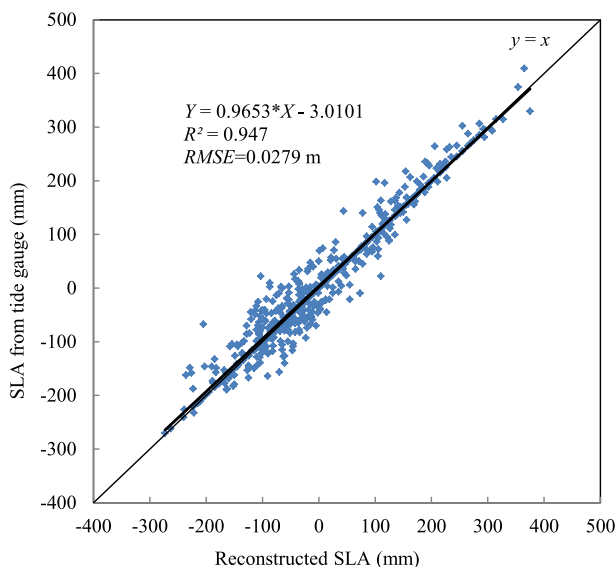


Fig. 5. Scatter diagram of comparison between the SLAs from Zhapo tide gauge and the nearest gridded reconstruction.

3.5. Analysis of sea level variability in the PRD

To estimate the long term trend of the sea level variability, a running average was computed with a one-year window to remove high frequency signals from the RCSLA (Fenoglio-Marc, 2002). A linear trend of 3.72 mm/yr was obtained from the remainder, as shown in Fig. 6. According to the ICE5-G (VM2) (Peltier, 2004), the Glacial Isostatic Adjustment (GIA) correction in this region was about -0.36 mm/yr. It implies that the relative sea level increases on the rate of 4.08 mm/yr during 1959–2011 in the PRD. Different results were obtained for sea level variability depending on the tide gauges used, the record lengths available, and the methods adopted in the investigation. The IPCC Fourth Assessment Report described global mean increases in sea level with trends of 1.8 ± 0.5 mm/yr and 3.1 ± 0.7 mm/yr for the periods 1961–2003 and 1993–2003, respectively (IPCC, 2007). Sea level change in the PRD over the period 1959–1988 may have been around 3.1 mm/yr (without GIA correction) (Yang et al., 1998). According to a 2010 report investigating sea level in China, the sea level around Guangdong Province has been rising at the speed of 2.5 mm/yr over the past 30 years (State Ocean Administration, 2011), and this is expected to increase to 2.6–4.3 mm/yr by 2040 (State Ocean Administration, 2013). Thus, the result presented here, which indicates sea level rise in the PRD with a linear trend of 4.08 mm/yr for the period 1959–2011, is broadly consistent with those of previous studies (You et al., 2012). Minor differences in estimates of sea level rise may have arisen from the use of more traditional methods in previous studies (e.g., the use of simple averaging techniques) in contrast to the PCA-based reconstruction adopted here, which analyzes the dominant spatial structures of sea level at the regional scale and can represent regional characteristics comprehensively.

4. Conclusions

To overcome the obstacles like the sparse of the tide gauge records and the short term coverage of satellite altimetry data, sea level anomalies of the PRD were reconstructed by combining the two datasets for the accurate long term trend estimation. EOF decomposition and the least-squares method were applied to create the RCSLA datasets for the period 1959–2011, with the same temporal resolution as satellite altimetry data and the same length as tide gauge records.

The comparison of spatial patterns from two parts of the satellite altimetry dataset produces high correlations, providing confidence in the hypothesis that the spatial structures of SLA can be used for the whole reconstruction period. Low RMSE and high R²

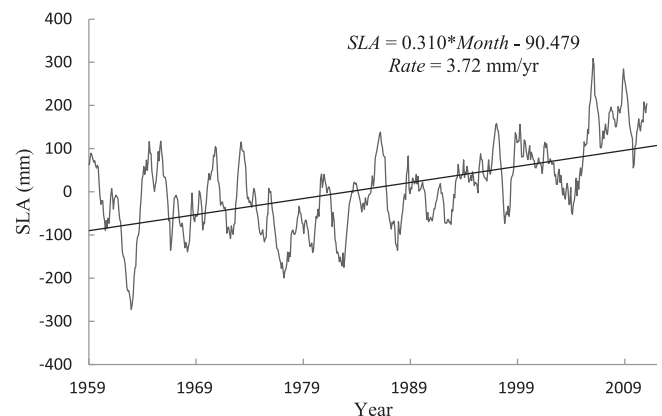


Fig. 6. Linear trend of sea level rise from RCSLA during 1959–2011. A 12-month running average has been applied.

value indicated the reconstruction shows a good performance, demonstrating the applicability of the method in regional sea level estimation. The results presented here also demonstrate that the accuracy of the reconstruction is not particularly sensitive to the length of the tide gauge records; therefore, even short and discontinuous records should be useful in the estimation of long-term sea level variability. The reconstruction addresses issues such as the relatively short term coverage of satellite altimetry data and the poor spatial resolution of the tide gauge records, implying the improvements of this method in the accurate estimation of long term regional sea level change.

The results from the reconstructed datasets show that the regional sea level has increased at a rate of 4.08 mm/yr over the period 1959–2011, and the annual and inter-annual cycles are the dominant variabilities in the PRD. The results also reveal that the spatial structures of sea level change are not uniform, the different patterns of variability in the river mouth and the coastline are the effects of the local factor river offs. The impacts of El Niño event can be observed in the main spatial structures of the sea level change. Some uncertainties in the reconstruction are largely owing to the discontinuous nature of the tide gauge records and so on.

Acknowledgements

This study was conducted under the auspices of the National Basic Research Program of China (973 Program, No. 2012CB95570002). Special thanks are due to the PSMSL and Guangdong Hydrology Bureau for providing the tide gauge data; the river flow time series were obtained from the Guangdong Hydrology Bureau. The altimetry products used in this study were produced by Ssalto/Duacs and distributed by AVISO, with support from the Centre National d'Etudes Spatiales (CNES).

References

- AVISO, 2013. SSALTO/DUACS User Handbook: (M)SLA and (M)ADT Near-real Time and Delayed Time Products.
- Barbosa, S.M., Fernandes, M.J., Silva, M.E., 2005. Space-time analysis of sea level in the North Atlantic from TOPEX/poseidon satellite altimetry. In: Jekeli, C., Bastos, L., Fernandes, J. (Eds.), *Gravity, Geoid and Space Missions*. Springer, Berlin Heidelberg, pp. 248–253.
- Barbosa, S.M., Silva, M.E., 2009. Low-frequency sea-level change in Chesapeake Bay: changing seasonality and long-term trends. *Estuar. Coast. Shelf Sci.* 83, 30–38.
- Becker, M., Meyssignac, B., Letetrel, C., Llovel, W., Cazenave, A., Delcroix, T., 2012. Sea level variations at tropical Pacific islands since 1950. *Global Planet. Change* 80–81, 85–98.
- Bi, H.S., Peterson, W.T., Strub, P.T., 2011. Transport and coastal zooplankton communities in the northern California current system. *Geophys. Res. Lett.* 38.
- Boateng, I., 2012. An assessment of the physical impacts of sea-level rise and coastal adaptation: a case study of the eastern coast of Ghana. *Clim. Change* 114, 273–293.
- Bosello, F., Nicholls, R.J., Richards, J., Roson, R., Tol, R.S.J., 2012. Economic impacts of climate change in Europe: sea-level rise. *Clim. Change* 112, 63–81.
- Bouffard, J., Roblou, L., Birol, F., Pascual, A., Fenoglio-Marc, L., Cancet, M., Morrow, R., Ménard, Y., 2011. Introduction and assessment of improved coastal altimetry strategies: case study over the Northwestern Mediterranean sea. In: Vignudelli, S., Kostianoy, A.G., Cipollini, P., Benveniste, J. (Eds.), *Coastal Altimetry*. Springer, Berlin Heidelberg, pp. 297–330.
- Calafat, F.M., Gomis, D., Marcos, M., 2009. Comparison of Mediterranean sea level fields for the period 1961–2000 as given by a data reconstruction and a 3D model. *Global Planet. Change* 68, 175–184.
- Calafat, F.M., Jorda, G., 2011. A Mediterranean sea level reconstruction (1950–2008) with error budget estimates. *Global Planet. Change* 79, 118–133.
- Cazenave, A., Bonnefond, P., Mercier, F., Dominh, K., Toumazou, V., 2002. Sea level variations in the Mediterranean Sea and Black Sea from satellite altimetry and tide gauges. *Global Planet. Change* 34, 59–86.
- Chambers, D.P., Mehlhaff, C.A., Urban, T.J., Nerem, R.S., 2002. Analysis of interannual and low-frequency variability in global mean sea level from altimetry and tide gauges. *Phys. Chem. Earth* 27, 1407–1411.
- Cheng, Y.C., Andersen, O.B., Knudsen, P., 2012. Integrating non-tidal sea level data from altimetry and tide gauges for coastal sea level prediction. *Adv. Space Res.* 50, 1099–1106.
- Church, J.A., White, N.J., Hunter, J.R., 2006. Sea-level rise at tropical Pacific and Indian Ocean islands. *Global Planet. Change* 53, 155–168.
- Chust, G., Caballero, A., Marcos, M., Liria, P., Hernandez, C., Borja, A., 2010. Regional scenarios of sea level rise and impacts on Basque (Bay of Biscay) coastal habitats, throughout the 21st century. *Estuar. Coast. Shelf Sci.* 87, 113–124.
- Dean, R.G., Houston, J.R., 2013. Recent sea level trends and accelerations: comparison of tide gauge and satellite results. *Coast. Eng.* 75, 4–9.
- Ding, X., Zheng, D., Chen, Y., Chao, J., Li, Z., 2001. Sea level change in Hong Kong from tide gauge measurements of 1954–1999. *J. Geodesy* 74, 683–689.
- Ducet, N., Le Traon, P.Y., Reverdin, G., 2000. Global high-resolution mapping of ocean circulation from TOPEX/poseidon and ERS-1 and-2. *J. Geophys. Research-Oceans* 105, 19477–19498.
- Escudier, R., Bouffard, J., Pascual, A., Poulain, P.-M., Pujol, M.-L., 2013. Improvement of coastal and mesoscale observation from space: application to the north-western Mediterranean Sea. *Geophys. Res. Lett.* 40, 2148–2153.
- Feng, W., Zhong, M., Xu, H.Z., 2012. Sea level variations in the South China Sea inferred from satellite gravity, altimetry, and oceanographic data. *Sci. China-Earth Sci.* 55, 1696–1701.
- Fenoglio-Marc, L., 2002. Long-term sea level change in the Mediterranean Sea from multi-satellite altimetry and tide gauges. *Phys. Chem. Earth* 27, 1419–1431.
- Gomez-Enri, J., Aboitiz, A., Tejedor, B., Villares, P., 2012. Seasonal and interannual variability in the Gulf of Cadiz: validation of gridded altimeter products. *Estuar. Coast. Shelf Sci.* 96, 114–121.
- Hallegratte, S., Green, C., Nicholls, R.J., Corfee-Morlot, J., 2013. Future flood losses in major coastal cities. *Nat. Clim. Change* 3, 802–806.
- Hamlington, B.D., Leben, R.R., Wright, L.A., Kim, K.Y., 2012. Regional sea level reconstruction in the Pacific ocean. *Mar. Geol.* 35, 98–117.
- Ho, C.R., Kuo, N.J., Zheng, Q.N., Soong, Y.S., 2000. Dynamically active areas in the South China Sea detected from TOPEX/Poseidon satellite altimeter data. *Remote Sens. Environ.* 71, 320–328.
- Holgate, S.J., Woodworth, P.L., 2004. Evidence for enhanced coastal sea level rise during the 1990s. *Geophys. Res. Lett.* 31.
- Huang, Z.G., Zhang, W.Q., Wu, H.S., Chen, T.G., Fan, J.C., Jiang, P.L., Li, Z.H., Huang, B.S., 2001. A prediction of sea level rising amplitude in 2030 and defensive countermeasures in the Zhujiang delta. *Sci. China Ser. D-Earth Sci.* 44, 446–454.
- Huang, Z.G., Zong, Y.Q., Zhang, W.Q., 2004. Coastal inundation due to sea level rise in the Pearl River Delta, China. *Nat. Hazards* 33, 247–264.
- IPCC, 2007. *Climate Change 2007: the Physical Science Basis. Contribution of Working Group I to the Fourth Assessment Report of the Intergovernmental Panel on Climate Change*. Cambridge University Press, Cambridge ; New York.
- Isern-Fontanet, J., Garcia-Ladona, E., Font, J., 2003. Identification of marine eddies from altimetric maps. *J. Atmos. Ocean. Technol.* 20, 772–778.
- Karim, M.F., Mimura, N., 2008. Impacts of climate change and sea-level rise on cyclonic storm surge floods in Bangladesh. *Global Environ. Change-Human Policy Dimensions* 18, 490–500.
- Latif, M., Barnett, T.P., 1994. Causes of decadal climate variability over the North Pacific and North-America. *Science* 266, 634–637.
- Le Traon, P.Y., Faugere, Y., Hernandez, F., Dorandeu, J., Mertz, F., Ablain, M., 2003. Can we merge GEOSAT follow-on with TOPEX/Poseidon and ERS-2 for an improved description of the ocean circulation? *J. Atmos. Ocean. Technol.* 20, 889–895.
- Le Traon, P.Y., Nadal, F., Ducet, N., 1998. An improved mapping method of multi-satellite altimeter data. *J. Atmos. Ocean. Technol.* 15, 522–534.
- Le Traon, P.Y., Ogor, F., 1998. ERS-1/2 orbit improvement using TOPEX/POSEIDON: the 2cm challenge. *J. Geophys. Res.-Oceans* 103, 8045–8057.
- Marcos, M., Tsimplis, M.N., Calafat, F.M., 2012. Inter-annual and decadal sea level variations in the north-western Pacific marginal seas. *Prog. Oceanogr.* 105, 4–21.
- Meyssignac, B., Calafat, F.M., Somot, S., Rupolo, V., Stocchi, P., Llovel, W., Cazenave, A., 2011. Two-dimensional reconstruction of the Mediterranean sea level over 1970–2006 from tide gage data and regional ocean circulation model outputs. *Global Planet. Change* 77, 49–61.
- Mitchum, G.T., 2000. An improved calibration of satellite Altimetric heights using tide gauge sea levels with adjustment for land motion. *Mar. Geod.* 23, 145–166.
- Nerem, R.S., Chambers, D.P., Leuliette, E.W., Mitchum, G.T., Giese, B.S., 1999. Variations in global mean sea level associated with the 1997–1998 ENSO event: Implications for measuring long term sea level change. *Geophys. Res. Lett.* 26, 3005–3008.
- Nerem, R.S., Leuliette, E., Cazenave, A., 2006. Present-day sea-level change: a review. *Comptes Rendus Geosci.* 338, 1077–1083.
- Nicholls, R.J., Cazenave, A., 2010. Sea-level rise and its impact on coastal zones. *Science* 328, 1517–1520.
- Niedzielski, T., Mizinski, B., 2013. Automated system for near-real time modelling and prediction of altimeter-derived sea level anomalies. *Comput. Geosci.* 58, 29–39.
- Parker, A., 2013. Sea level trends at locations of the United States with more than 100 years of recording. *Nat. Hazards* 65, 1011–1021.
- Parker, B.B., 1991. Sea-level as an indicator of climate and global change. *Mar. Technol. Soc. J.* 25, 13–24.
- Parkinson, R.W., McCue, T., 2011. Assessing municipal vulnerability to predicted sea level rise: city of satellite beach, Florida. *Clim. Change* 107, 203–223.
- Pascual, A., Faugere, Y., Larnicol, G., Le Traon, P.Y., 2006. Improved description of the ocean mesoscale variability by combining four satellite altimeters. *Geophys. Res. Lett.* 33.
- Peltier, W.R., 2004. Global glacial isostasy and the surface of the ice-age earth: the ice-5G (VM2) model and grace. *Annu. Rev. Earth Planet. Sci.* 32, 111–149.
- Pendleton, L., King, P., Mohn, C., Webster, D.G., Vaughn, R., Adams, P.N., 2011. Estimating the potential economic impacts of climate change on Southern California beaches. *Clim. Change* 109, 277–298.

- Penduff, T., Juza, M., Brodeau, L., Smith, G.C., Barnier, B., Molines, J.M., Treguier, A.M., Madec, G., 2010. Impact of global ocean model resolution on sea-level variability with emphasis on interannual time scales. *Ocean. Sci.* 6, 269–284.
- Prandi, P., Cazenave, A., Becker, M., 2009. Is coastal mean sea level rising faster than the global mean? A comparison between tide gauges and satellite altimetry over 1993–2007. *Geophys. Res. Lett.* 36.
- Preisendorfer, R.W., Mobley, C.D., 1988. *Principal Component Analysis in Meteorology and Oceanography*. Elsevier, Amsterdam, p. 436.
- Raicich, F., 2008. A review of sea level observations and low frequency sea-level variability in South Atlantic. *Phys. Chem. Earth* 33, 239–249.
- Ren, M.E., 1993. Relative sea-level changes in China over the last 80 years. *J. Coast. Res.* 9, 229–241.
- Rong, Z.R., Liu, Y.G., Zong, H.B., Xiu, P., 2009. Long term sea level change and water mass balance in the South China Sea. *J. Ocean. Univ. China* 8, 327–334.
- Ryan, H.F., Noble, M.A., 2007. Sea level fluctuations in central California at subtidal to decadal and longer time scales with implications for San Francisco Bay, California. *Estuar. Coast. Shelf Sci.* 73, 538–550.
- Siedler, G., Rouault, M., Lutjeharms, J.R.E., 2006. Structure and origin of the subtropical South Indian Ocean countercurrent. *Geophys. Res. Lett.* 33.
- Smith, T.M., Reynolds, R.W., Livezey, R.E., Stokes, D.C., 1996. Reconstruction of historical sea surface temperatures using empirical orthogonal functions. *J. Clim.* 9, 1403–1420.
- Stanev, E.V., Peneva, E.L., 2001. Regional sea level response to global climatic change: Black Sea examples. *Global Planet. Change* 32, 33–47.
- State Ocean Administration, PRC, 2011. 2010 Report on China's Sea Level. WWW Pages. http://www.soa.gov.cn/zwgk/hygb/zghpmgb/2010nzghpmgb/201212/t20121217_22808.html.
- State Ocean Administration, PRC, 2013. 2012 Report on China's Sea Level. WWW Pages. http://www.soa.gov.cn/zwgk/hygb/zghpmgb/2012nzghpmgb/201303/t20130307_24283.html.
- Unnikrishnan, A.S., Shankar, D., 2007. Are sea-level-rise trends along the coasts of the north Indian Ocean consistent with global estimates? *Global Planet. Change* 57, 301–307.
- VijayaVenkataRaman, S., Iniyan, S., Goic, R., 2012. A review of climate change, mitigation and adaptation. *Renew. Sustain. Energy Rev.* 16, 878–897.
- Weiss, J.L., Overpeck, J.T., Strauss, B., 2011. Implications of recent sea level rise science for low-elevation areas in coastal cities of the conterminous USA. *Clim. Change* 105, 635–645.
- Willis, J.K., Roemmich, D., Cornuelle, B., 2004. Interannual variability in upper ocean heat content, temperature, and thermocline expansion on global scales. *J. Geophys. Res.-Oceans* 109.
- Woodroffe, C.D., Murray-Wallace, C.V., 2012. Sea-level rise and coastal change: the past as a guide to the future. *Quat. Sci. Rev.* 54, 4–11.
- Woodworth, P.L., Player, R., 2003. The permanent service for mean sea level: an update to the 21st century. *J. Coast. Res.* 19, 287–295.
- Xie, Z.R., Yuan, L.W., Lv, G.N., 2012. Sea Level-land Surface System Chang: Reconstruction. Monitoring. Estimation. Science Press, Beijing, p. 370 (in Chinese).
- Yang, Q.S., Luo, Z.R., Zhang, X.J., 1998. Secular trend of water level change in Zhujiang River Delta in recent decades. *Trop. Oceanol.*, 9–14 (in Chinese, with English abstract).
- Yin, J., Yu, D.P., Yin, Z.N., Wang, J., Xu, S.Y., 2013. Modelling the combined impacts of sea-level rise and land subsidence on storm tides induced flooding of the Huangpu River in Shanghai, China. *Clim. Change* 119, 919–932.
- You, D.W., Tang, C.L., Chen, T.G., Cai, B., Yu, K.F., 2012. Sea level changes along Guangdong coast over the last century. *Trop. Geogr.*, 1–5 (in Chinese, with English abstract).
- Zuo, J.C., Yang, Y.Q., Zhang, J.L., Chen, M.X., Xu, Q., 2013. Prediction of china's submerged coastal areas by sea level rise due to climate change. *J. Ocean. Univ. China* 12, 327–334.